Nine-Frequency-Path Quantum Interferometry over 60 km of Optical Fiber

Batiste Galmès[1], Kien Phan-Huy[1], Luca Furfaro[1], Yanne K. Chembo[2,3],* and Jean-Marc Merolla[1†]
[1] *FEMTO-ST Institute, Univ. Bourgogne Franche-Comté, CNRS, Optics Department, 15B Avenue des Montboucons, 25030 Besançon cedex, France.*
[2] *GeorgiaTech-CNRS Joint International Laboratory [UMI 2958], Atlanta Mirror Site, School of Electrical and Computer Engineering, 777 Atlantic Dr NW, Atlanta GA 30332, USA.*
[3] *Now at the Institute for Research in Electronics and Applied Physics (IREAP), and at the Department of Electrical and Computer Engineering, University of Maryland, College Park MD 20742, USA.*
(Dated: January 18, 2019)

The archetypal quantum interferometry experiment yields an interference pattern that results from the indistinguishability of two spatiotemporal paths available to a photon or to a pair of entangled photons. A fundamental challenge in quantum interferometry is to perform such experiments with a higher number of paths, and over large distances. We demonstrate that using indistinguishable frequency paths instead of spatiotemporal ones allows for robust, high-dimensional quantum interferometry in optical fibers. In our system, twin-photons from an Einstein-Podolsky-Rosen (EPR) pair are offered up to 9 frequency paths after propagation in long-haul optical fibers, and we show that the multi-path quantum interference patterns can be faithfully restored after the photons travel a total distance of up to 60 km.

I. INTRODUCTION

Quantum information networks require the manipulation and transportation of entangled photons in long-haul optical fiber networks without destroying their non-classical correlations. The relevance and viability of any prospective quantum network also critically depends on a strong hardware overlap with off-the-shelf components, readily available in the technologically mature sector of optical fiber telecommunications. Fulfilling these constraints while preserving the non-classical correlations of entangled photons when launched in long-haul optical fibers arises as particularly difficult task, and even more so if the entanglement is high-dimensional.

We present here a proof-of-concept quantum interferometry experiment in which high-dimensional quantum entanglement is preserved even after the photons have propagated in long-haul optical fibers. We report a long-distance nonlocal interference experiment based on frequency domain interferometric scheme using electro-optic phase modulators, in which nonlocal dispersion cancellation is performed. The electro-optic phase modulators leading to N frequency paths instead of the two temporal in the typical Franson interferometer. As N-frequency paths are involved, the dispersion strongly affects the interference pattern and leads to radically different observations. We show that the dispersion not only alters the visibility but also disturbs the shape of the interference pattern and we demonstrate how the effect of the dispersion can be cancelled non-locally. This preliminary results confirm also that the high-dimensional quantum entanglement is preserved even after the photons have propagated in long-haul optical fibers.

The paper is divided into three main parts. We first describe our experiment and we present the effects of the dispersion on the N-frequency path interferences. In the second part, we propose a theoretical analysis of the system, and outline the formalism use to quantify the quantum correlations. The last part presents our main experimental result, in which multi-path quantum interference patterns can be faithfully restored after the photons travel a total distance of up to 60 km, in good agreement with the theoretical predictions.

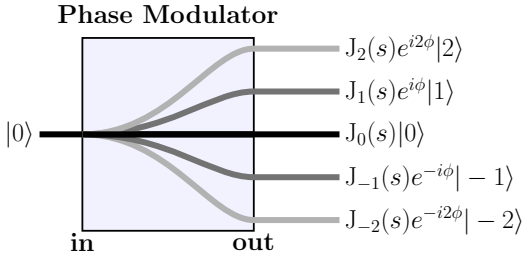

FIG. 1: Principle of multiple frequency paths using a phase modulator seeded with a photon of frequency ω_0. The modulator is driven by a sinusoidal RF signal of amplitude sV_π, frequency Ω and phase ϕ. This modulation creates the eigenstates $|n\rangle \equiv |\omega_0 + n\Omega\rangle$ with $n \in \mathbb{Z}$, which are new frequency paths available with probability $\mathrm{J}_n^2(s)$ to any incoming photon in the eigenstate $|0\rangle$. Only 5 eigenstates are represented here for clarity, but the entangled photons explore up to 9 frequency paths in our experimental transmission system. Along with robustness, this high dimensionality is a distinctive advantage of frequency path quantum interferometry in comparison to spatiotemporal schemes.

*ykchembo@umd.edu
†jeanmarc.merolla@univ-fcomte.fr

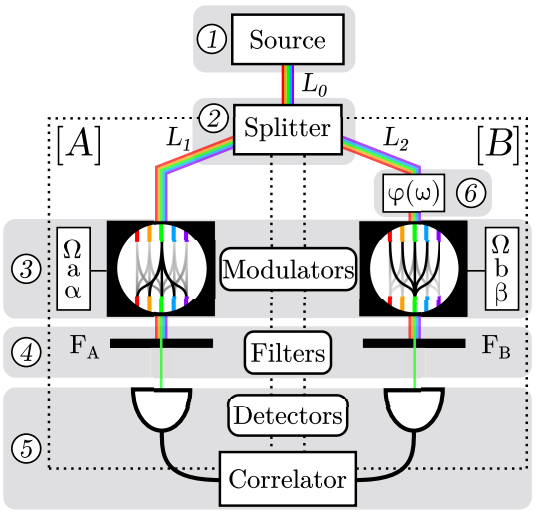

FIG. 2: Schematic representation of the experimental setup. (1) Broadband twin-photon source. (2) 3 dB splitter towards arms $[A]$ and $[B]$. (3) Phase modulators providing the frequency paths. (4) Bragg filters to select the output photon pairs. (5) Detection and correlation. (6) Dispersion compensation system.

II. EXPERIMENTAL SYSTEM

Our system is based on the idea of Franson interferometry [1]. We pump a 3 cm-long periodically poled lithium niobate (PPLN) waveguide around 775 nm to generate entangled photons via spontaneous parametric down conversion (SPDC) around $\lambda_0 = 2\pi c/\omega_0 = 1550$ nm. The spectral density $f(\omega)$ of this source spans over $\sim 2\pi \times 12$ THz around ω_0 (~ 100 nm around λ_0), and the quantum state of the twin-photons is

$$|\psi\rangle = \int_{-\infty}^{+\infty} d\omega f(\omega)|\omega_0 - \omega\rangle|\omega_0 + \omega\rangle\,. \tag{1}$$

The entangled photons are then launched into a standard SMF-28 fiber of length L_0 before being separated by a 3 dB coupler in two arms $[A]$ (Alice) and $[B]$ (Bob).

Each arm includes another fiber spool of length $L_{A,B}$, which transform the input state after propagation into

$$|\psi\rangle = \int_{-\infty}^{+\infty} d\omega f(\omega) e^{i\Phi(\omega)}|\omega_0 + \omega\rangle_A|\omega_0 - \omega\rangle_B \tag{2}$$

where

$$\Phi(\omega) = \beta(\omega)[L_0 + L_A] + \beta(-\omega)[L_0 + L_B] \tag{3}$$

denotes the phase shift resulting from the propagation in the optical fibers $L_{0,A,B}$, and $\beta(\omega)$ represents the corresponding fiber dispersion. Whereas Franson interferometry usually involves Mach-Zehnder (MZ) modulators offering two temporal paths [2–5], our system exploits instead $N \gg 2$ frequency paths offered by phase modulators (PM) [6–8]. The creation of these frequency paths is performed using two phase modulators $\mathrm{PM}_{A,B}$ of half-wave voltage V_π, modulated at the frequency $\Omega/2\pi = 12.5$ GHz with signals of normalized amplitudes $\{a, b\} = V_{\{a,b\}}/V_\pi$ and phases $\{\varphi_A, \varphi_B\}$.

III. THEORETICAL ANALYSIS

The modulators $\mathrm{PM}_{A,B}$ induce the transformations

$$|n\rangle_{A,B} \to \sum_{k\in\mathbb{Z}} \mathrm{J}_k(\{a,b\}) e^{ik(\{\varphi_A,\varphi_B\}-\pi/2)}|n+k\rangle_{A,B}\,, \tag{4}$$

where

$$|n\rangle \equiv |\omega_0 + n\Omega\rangle \tag{5}$$

are new frequency paths with $n \in \mathbb{Z}$. As explained in Fig. 1, every path $|n\rangle$ is accessed with probability $\mathrm{J}_n^2(s)$ where $s \in \{a, b\}$ is the real-valued modulation index of the modulator. The closure condition

$$\sum_{n=-\infty}^{+\infty} \mathrm{J}_n^2(s) = 1 \tag{6}$$

is a property of Bessel functions and holds for all s. However, the probabilities $\mathrm{J}_n^2(s)$ decay rapidly to 0 as $n \to \pm\infty$, and only $N \simeq 2(s+1)+1$ frequency paths have a non-negligible probability. In our experimental setup, we have $s \simeq 3$ and accordingly, up to $N = 9$ paths with $n \in \{-4, \ldots, 4\}$ can be explored by the twin-photons. We use the two Bragg filters $F_{A,B}$ of bandwidth $\Omega_F/2\pi = 3$ GHz, which are respectively centered to $\omega_0 + n\Omega$ and $\omega_0 - n\Omega$.

Since the modulators sift the angular frequency by Ω, it is convenient to expand following the frequency-bin decomposition

$$\begin{aligned}|\psi\rangle \;=\; & \int_{-\Omega/2}^{+\Omega/2} d\omega \sum_{k=-\infty}^{+\infty} f(\omega + k\Omega) \\ & \times |\omega_0 - \omega - k\Omega\rangle|\omega_0 + \omega + k\Omega\rangle\,.\end{aligned} \tag{7}$$

On the other hand, the phase shift for a photon in a state $|\omega\rangle$ after propagation in a length L of optical fiber can be explicitly expressed as

$$|\omega\rangle_{\mathrm{out}} = e^{i\beta(\omega)L}|\omega\rangle_{\mathrm{in}}\,. \tag{8}$$

As a consequence, the probability of coincidence measurement by the avalanche photodetectors D_A and D_B is therefore

$$P_n = \left| \int_{-\Omega/2}^{+\Omega/2} \mathrm{d}\omega\, g_n(\omega) \sum_{k\in\mathbb{Z}} \mathrm{J}_k(a)\mathrm{J}_{-k}(b) e^{-i\Phi(k,n,\omega)} \right|^2, \tag{9}$$

where

$$\begin{aligned}\Phi(k,n,\omega) \;=\; & k\left(\Delta\varphi + \beta_1\Omega\Delta L\right) \\ & -k\left(\mu + \frac{1}{2}\beta_2 L\right)(\omega + n\Omega)\Omega \\ & +k^2\Omega^2\left(\mu + \frac{1}{2}\beta_2 L\right)\end{aligned} \tag{10}$$

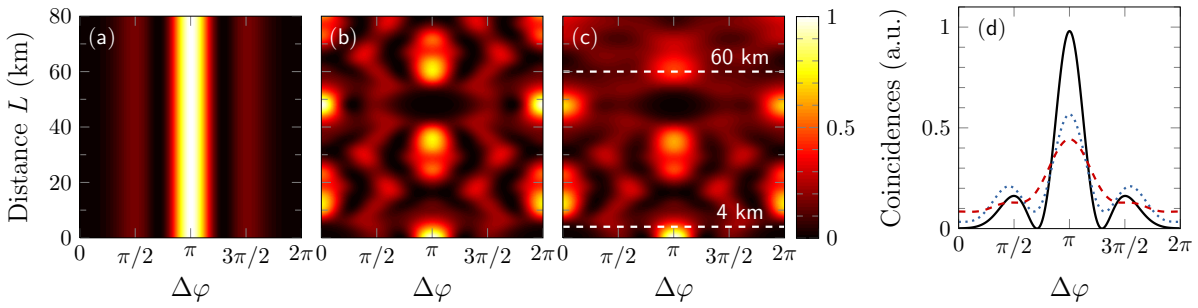

FIG. 3: Numerical simulation of the interference patterns with respect to the total distance L traveled by the twin-photons, using Eq. (9). The parameters are $a = b = 2.75$, $\Delta L = 0$, and the filters are positioned at $n = 0$. (a) Ideal case with no dispersion ($\beta_2 = 0$) and perfectly monochromatic filters ($\Omega_F = 0$). The interference pattern [which corresponds to the continuous black line in Fig. 3(d)] remains unaffected by the propagation. (b) Case where dispersion is accounted for ($\beta_2 = -22$ ps^2/km) but the filters are still perfectly monochromatic. The interference pattern evolves periodically, with a period L_p corresponding to length necessary for the accumulated dispersion phase $\beta_2\Omega^2 L_p/2$ to amount to 2π. (c) Realistic case where both the dispersion and the bandwidth of the Bragg filters ($\Omega_F/2\pi = 3$ GHz) are accounted for. The interference pattern is irreversibly altered during propagation and impedes long-haul quantum interferometry. (d) Quantum interference patterns from Fig. 3(c) at $L = 0$ km (continuous black), $L = 4$ km (dotted blue), and $L = 60$ km (dashed red).

up to second-order dispersion termes. In the above equation, β_1 and β_2 are respectively the group velocity and the group velocity dispersion in the optical fibers, $L = 2L_0 + L_A + L_B$ the total distance traveled by the twin-photons, $\Delta L = L_B - L_A$ the distance mismatch, $g_n(\omega)$ is spectral density of the source after being altered by the Bragg elements and the propagation along the optical fibers, while μ is the quadratic (second-order) coefficient of the dispersion compensation module. The superposition of indistinguishable paths as given by the summation over k, and squaring the sum gives rise to quantum interferences. The two-photon interference patterns are obtained by scanning the phase difference $\Delta\varphi = \varphi_B - \varphi_A$. Since the filters have a finite bandwidth Ω_F, the integration of ω over $[-\Omega_F/2, \Omega_F/2]$ results in a continuous superposition of shifted interference patterns leading to a loss of visibility.

The dispersion phase-shift $\Phi(k, n, \omega)$ is such that the β_1-induced shift is easily canceled with the matching $L_A = L_B$, while the dispersion-induced shift cannot except when the dispersion cancellation is emulated via $\mu = -\frac{1}{2}\beta_2 L$. This phenomenon is illustrated in Fig. 3 which shows the evolution of numerically simulated interference patterns as the twin-photons propagate in the optical fibers. It can be seen that dispersion not only alters the visibility of the fringes, but also disturbs the shape of the interference pattern – and thus, the quantum correlations.

It should be noted that this result is essentially different from conventional time-based system using a Mach-Zehnder modulator [21]. In that case, a sine interference pattern is measured because it involves the superposition of two temporal paths. As the dispersion only affects the phase relationship between the two paths, a superposition of shifted sine patterns is obtained leading to a visibility loss. On the contrary, our method involves the interference of N paths to produce a Bessel-like interference pattern. As the dispersion affects the phase relationship between all the N paths, the interference is strongly altered as shown by Fig. 3. Another consequence is that the time-based MZ experiment is positively sensitive to source filtering. As reported in ref. [21], if one uses a narrowband filter to turn the propagation from "impulse" to "continuous-wave", it will isolate one sine interference pattern from the superposition, and reduce effectively the dispersion effects. In our frequency-path system, one can not reduce the source bandwidth to limit the effect of dispersion, and furthermore, the use of $N \gg 2$ frequency paths leads to a strong deformation of the interference pattern that adds to the visibility loss. This is why an efficient dispersion cancellation strategy is an absolute requirement for this frequency-path interferometric approach.

Indeed, unlike in the classical case, the problem of dispersion cancellation in the context of quantum interferometry is not conceptually trivial, as dispersion can be canceled either *locally* [9–17] or *nonlocally* [18–21]. Research is still on-going about the classical or quantum nature of the non-local dispersion approach [22, 23].

Dispersion cancellation in two-photon experiments was simultaneously introduced in 1992 by Steinberg *et al.* [9] and Franson [18]. Steinberg *et al.* proposed a dispersion cancellation scheme based on a Hong-Ou-Mandel interferometer in which photons are recombined through a beam splitter before detection [24]. Conversely, Franson proposed a nonlocal dispersion scheme in which separated photons experienced independently dispersion effects of opposite-signs without recombination before detection. These seminal papers introduced a debate about the classical or quantum nature of the dispersion cancellation [22, 25] stimulating the development of classical experiments [20, 26], producing comparable results to those predicted by Steinberg *et al.* and Franson. However, Franson demonstrated the inability of classical models

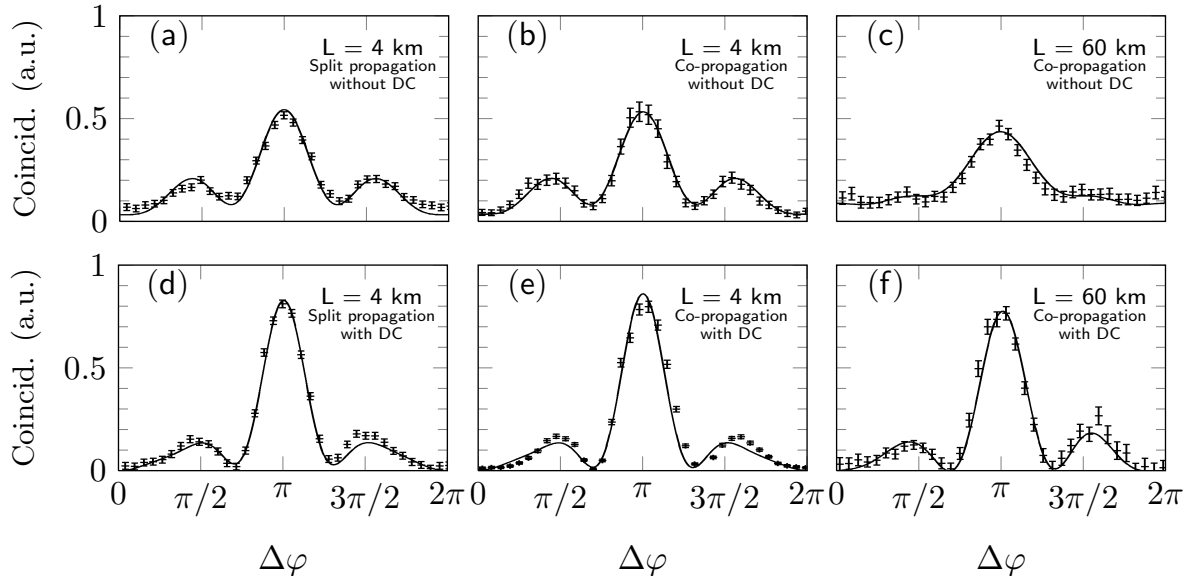

FIG. 4: Experimental measurements of the normalized coincidences as a function of the phase difference $\Delta\varphi$, for moderate (4 km) and long (60 km) distance propagation. The upper row (a)–(c) corresponds to experimental results without any dispersion compensation (DC), while the lower row (d)–(f) corresponds to measurements performed when the nonlocal dispersion compensation scheme is implemented. The theoretical Bessel-like patterns are the continuous lines, while the experimental results are indicated with the symbols. (a) and (d): Interference patterns for 2 km split propagation in L_A and L_B ($L = L_A + L_B \simeq 4$ km) (b) and (e): Interference patterns for 2 km co-propagation in L_0 ($L = 2L_0 \simeq 4$ km). (c) and (f): Interference patterns for 30 km co-propagation in L_0 ($L = 2L_0 \simeq 60$ km).

to describe all of the relevant aspects of nonlocal dispersion [19]. Different experimental set-ups have been proposed to explore nonlocal dispersion cancellation such as nonlocal interferometry or even non-interferometric architectures as suggested by Franson [19]. The sources in that case can be based on spectral [17] or angular-momentum entanglement [16].

Our method requires a minimum bandwidth to allow the N-frequency paths: it is therefore not only sensitive to dispersion by nature, but it actually needs the dispersion to be *nonlocal*. We show here that the dispersion can be canceled non-locally, thereby restoring the original interference pattern after the twin-photons are propagated in long-haul optical fibers. When $L_A = L_B$, the dispersion shift $\Phi(k, n, \omega)$ depends only the total propagation distance $L = 2L_0 + L_A + L_B$ traveled by the twin-photons. In fact, the dispersion effect is the same whether both photons co-propagate along the fiber (L_0), or only along one of the two arms ($L_{A,B}$). This has two major consequences. First, the whole propagation and dispersion can actually be experienced by only one photon and still lead to the same measurements. Second, a negative dispersion applied anywhere cancels the effect. To perform nonlocal dispersion cancellation, a dispersion-compensation module (DCM) is inserted in arm $[A]$, as shown in Fig. 2. This module introduces a negative phase-shift that compensates to the group velocity dispersion phase shift. The coincidence probability of Eq. (9) becomes

$$P_n \propto |\mathrm{J}_0(c)|^2 \;\text{ with }\; c = [a^2 + b^2 + 2ab\cos(\Delta\varphi)]^{\frac{1}{2}} \,, \quad (11)$$

so that the initial Bessel-like interference pattern is fully recovered [5].

IV. RESULTS

The experimental results are presented in Fig. 4. The acquisition of the interference patterns required stable continuous operation for several days. In particular, each interference pattern corresponds to continuous data acquisition for a duration of 48 h. Photon counting was performed using LynXéa photon counters from Aurea Technology with onboard time-correlator. The filtering was performed using fiber-Bragg gratings (FBGs) with a full width at half-maximum (FWHM) bandwidth of 2.6 GHz, with more than 30 dB isolation at 5.6 GHz offset. This FBG filters are cascaded with circulators, and yielded overall losses around 1.5 dB. The bias voltages of the modulators are set with a precision of 100 μV.

Although full automation provides strong performances and reliability, large distances propagation features specific technical challenges. One of the most important difficulty comes from the phase-shift $\beta_1 \Delta L$ that shifts the interference pattern in $\Phi(k, n, \omega)$, since ΔL cannot be strictly set to 0 when $L_{A,B}$ is km-long. Indeed, for

large distances, this term is very sensitive to temperature as 1 K induces a 2π phase-shift per kilometer. A simple way to overcome this difficulty is to propagate most of the distance without separating the photons, split them and cancel the whole dispersion afterward. Consequently, ΔL is then nulled with the best precision possible, and the temperature fluctuations automatically are compensated for being the same for the twin-photon pair. The expected results are identical to the case in which the photons are first separated and then propagate most of the distance in two identical fibers $L_A \simeq L_B$. However, this solution may rise questions with regard to the actual separation of the photons and the "nonlocality" of the experiment. For this reason, two sets of experiments were performed.

We first let the photons propagate together in the same fiber $L_0 = 2$ km with negligible propagation in the arms $[A]$ and $[B]$ (with $L_A = L_B \simeq 0$). The results are then compared to the experiment in which the photons are separated right after the source ($L_0 \simeq 0$), while propagating over $L_A = L_B = 2$ km. In both cases, the total distance traveled by the twin photons is $L = 4$ km. A Finisar WaveShaper 4000S with 10 GHz resolution is used on arm $[A]$ to compensate for the dispersion, and Figs. 4(a) and (b) show how the Bessel interference pattern is restored for both experiments, in excellent agreement with the simulations. This confirms the fact that co-propagation (along L_0) or split propagation (along L_A and L_B) of the photon pair yield the same results, and as predicted by the theory, the visibility of the interference pattern is also restored.

Since co-propagation or split propagation eventually results in the same outcome, a second set of experiments was performed. Here, in order to show our ability to cancel the dispersion over large distances, both photons travel together within the same fiber of length $L_0 = 30$ km while $L_A = L_B \simeq 0$, corresponding to a total distance $L = 60$ km for the twin-photons. The Finisar DCM is replaced by a DCMX from Teraxion with fixed dispersion cancellation for 60 km. The results are shown in Figure 4(c). One can note a slight dissymmetry between the two Bessel side-lobes in the experimental data, and it originates from the DCM limited bandwidth. However, once the DCM response is accounted for in our simulation, an excellent agreement is achieved for the case of long-haul fiber propagation.

V. CONCLUSION

In conclusion, we have demonstrated robust, high-dimensional ($N = 9$) frequency-path quantum interferometry in long-haul optical fibers, in which twin-photons travel a distance up to 60 km. We expect such systems to play a major role in future quantum information networks, particularly for quantum-key distribution frequency-based systems [6, 27]. It is also known that ultra-high Q whispering-gallery mode resonators are ideal platforms to achieve both high-capacity optical fiber communications [28] and quantum entanglement via the nonlinearity of the bulk material [29–31], and consequently, we expect as well our interferometric results to be relevant in the context of resonator-based quantum frequency combs [32, 33].

Acknowledgment

The authors would like to acknowledge fruitful interactions with Matthieu Bloch. This research has been funded by the Labex ACTION. It has also been funded by the projects CORPS, IQUINS, and PHYFA of the *Région Bourgogne Franche-Comté* in France.

[1] J. D. Franson, Phys. Rev. A **44**, 4552–4555 (1991).
[2] S. E. Harris, Phys. Rev. A **78**, 021807 (2008).
[3] S. Sensarn, G. Y. Yin, and S. E. Harris, Phys. Rev. Lett. **103**, 163601 (2009).
[4] L. Olislager, J. Cussey, A. T. Nguyen, P. Emplit, S. Massar, J.-M. Merolla, and K. P. Huy, Phys. Rev. A **82**, 013804 (2010).
[5] L. Olislager, I. Mbodji, E. Woodhead, J. Cussey, L. Furfaro, P. Emplit, S. Massar, K. P. Huy, and J.-M. Merolla, New Journal of Physics **14**, 043015 (2012).
[6] M. Bloch, S. W. McLaughlin, J.-M. Merolla, and F. Patois, Opt. Lett. **32**, 301–303 (2007).
[7] L. Olislager, E. Woodhead, K. P. Huy, J.-M. Merolla, P. Emplit, and S. Massar, Phys. Rev. A **89**, 052323 (2014).
[8] P. Imany, O. D. Odele, J. A. Jaramillo-Villegas, D. E. Leaird, and A. M. Weiner, Phys. Rev. A **97**, 013813 (2018).
[9] A. M. Steinberg, P. G. Kwiat, and R. Y. Chiao, Phys. Rev. Lett. **68**, 2421–2424 (1992).
[10] A. M. Steinberg, P. G. Kwiat, and R. Y. Chiao, Phys. Rev. A **45**, 6659–6665 (1992).
[11] K. A. O'Donnell, Phys. Rev. Lett. **106**, 063601 (2011).
[12] A. Cuevas, G. Carvacho, G. Saavedra, J. Cariñe, W. a. T. Nogueira, M. Figueroa, A. Cabello, P. Mataloni, G. Lima, and G. B. Xavier, Nat. Comm. **4** (2013).
[13] J. M. Lukens, A. Dezfooliyan, C. Langrock, M. M. Fejer, D. E. Leaird, and A. M. Weiner, Phys. Rev. Lett. **111**, 193603 (2013).
[14] T. Shirai and A. T. Friberg, J. Opt. Soc. Am. A **31**, 258–263 (2014).
[15] J. Brendel, H. Zbinden, and N. Gisin, Opt. Comm. **151**, 35–39 (1998).
[16] S. Cialdi, D. Brivio, E. Tesio, and M. G. A. Paris, Phys. Rev. A **84**, 043817 (2011).
[17] S.-Y. Baek, Y.-W. Cho, and Y.-H. Kim, Opt. Express **17**, 19241–19252 (2009).
[18] J. D. Franson, Phys. Rev. A **45**, 3126–3132 (1992).

[19] J. D. Franson, Phys. Rev. A **80**, 032119 (2009).
[20] V. Torres-Company, H. Lajunen, and A. T. Friberg, New Journal of Physics **11**, 063041 (2009).
[21] T. Zhong and F. N. C. Wong, Phys. Rev. A **88**, 020103 (2013).
[22] J. H. Shapiro, Phys. Rev. A **81**, 023824 (2010).
[23] J. D. Franson, Phys. Rev. A **81**, 023825 (2010).
[24] C. K. Hong, Z. Y. Ou, and L. Mandel, Phys. Rev. Lett. **59**, 2044–2046 (1987).
[25] K. J. Resch, P. Puvanathasan, J. S. Lundeen, M. W. Mitchell, and K. Bizheva, Opt. Express **15**, 8797–8804 (2007).
[26] R. Kaltenbaek, J. Lavoie, D. N. Biggerstaff, and K. J. Resch, Nat. Physics **4**, 864–868 (2008).
[27] J.-M. Merolla, Y. Mazurenko, J.-P. Goedgebuer, and W. T. Rhodes, Phys. Rev. Lett. **82**, 1656–1659 (1999).
[28] J. Pfeifle *et al.* Phys. Rev. Lett. textbf114, 093902 (2015)
[29] Y. K. Chembo, Nanophotonics **5**, 214 (2016).
[30] G. Lin, A. Coillet and Y. K. Chembo, Adv. Opt. Phot. **9**, 828 (2017).
[31] A. Pasquazi *et al.*, Phys. Rep. **729**, 1 (2018).
[32] Y. K. Chembo, Phys. Rev. A **93**, 033820 (2016).
[33] M. Kues *et al.*, Nature **546**, 622–626 (2017).